Int. J. Heat Mass Transfer. Vol. 29, No. 11, pp. 1723–1740, 1986
Printed in Great Britain

0017–9310/86 $3.00 + 0.00
Pergamon Journals Ltd.

Measurements and visualizations of transient and steady-state vertical natural convection flow in cold water

YOGENDRA JOSHI† and BENJAMIN GEBHART‡

† Department of Mechanical Engineering, Naval Postgraduate School, Monterey, CA 93943, U.S.A.
‡ Department of Mechanical Engineering and Applied Mechanics, University of Pennsylvania, Philadelphia, PA 19104, U.S.A.

(*Received* 10 *October* 1985 *and in final form* 14 *March* 1986)

Abstract—Results of an experimental investigation of transient natural convection flow and transport development adjacent to a suddenly heated, 1.27-m-high, vertical surface in cold water are given. These measurements determine the effects of the anomalous behavior of cold water on transient convective response and on the eventual steady-state heat transfer characteristics. The range of ambient temperatures studied is $1.2 \leqslant t_\infty \leqslant 6.8°C$, for surface heating rates in the range 587–1870 W m^{-2}. The transient and resulting eventual flows were visualized and local surface temperatures measured. For the lowest ambient temperature and heating conditions, $t_\infty = 1.2°C$ and 587 W m^{-2}, the established flow resembled a downward flowing boundary layer. As t_∞ and the heating rate are increased, the flow is not of simple boundary region form. A vigorous turbulent downflow, away from the surface, and intermittent upflow, very near the surface, was seen. Further increase in t_∞ and heating rate results in yet stronger inner upflows. The outer downflow existed at all times. However, it arose only intermittently for $t_\infty = 3.1°C$ and heating rates of 1140 and 1870 W m^{-2}. For these conditions, the flows resembled an upward flowing boundary layer. These changes in transport regime are confirmed by local surface temperature measurements. Surface height-averaged temperature, t_L, was used in the evaluation of Nu_L and Gr_L near the extremum temperature t_m. Average steady-state heat transfer data are best correlated by $Nu_L/Gr_L^{1/4} = 1.35|R-0.26|^{0.165}$ outside $0.23 < R < 0.29$, where $R = (t_m - t_\infty)/(t_L - t_\infty)$. Within $0.23 < R < 0.29$ a minimum in heat transfer rate is observed. Details of flow and transport evolution during the transient, starting from quiescence were also studied. Early one-dimensional conduction transport is followed by entrainment development. Both unidirectional and bidirectional entrainment development were seen, depending upon the ambient and surface-heating conditions. Bidirectional transient flows were found to be unstable, resulting eventually in turbulent flow. Transition to turbulence occurred simultaneously at all downstream distances. The persistence of one-dimensional transport was determined, at various downstream locations, for all ambient and heating conditions. The measurements show the qualitative changes in flow regimes and also the actual variation of the Nusselt number in the density extremum region. These characteristics are quite different from those found in the well-studied Boussinesq behavior.

1. INTRODUCTION

NATURAL convection flows in water near the density extremum temperatures abound in environment and technology. Reversals in the direction of buoyancy force and fluid velocity often occur. Such convective motions have been studied quite extensively, in the steady state; earlier investigations are summarized in Gebhart and Mollendorf [1] and a general method for analyzing such flows is suggested there, employing the cold water density formulation of Gebhart and Mollendorf [2]. Convective motions in ice melting are described by Carey and Gebhart [3].

Relatively few experimental studies have been made of purely thermally buoyant flows resulting from heating cold ambient water. Ede [4] made overall heat transfer measurements in cold water at t_∞, adjacent to a 10.2-cm-high, electrically heated surface. Surface temperatures, t_o, were measured for three conditions: (a) t_o and $t_\infty < 4°C$; (b) $t_o > 4°C > t_\infty$; and (c) t_o and $t_\infty > 4°C$. Heat transfer data were compared with the integral method boundary-layer analysis of Merk [5]. The flow behavior was not visualized.

Schechter and Isbin [6] used an integral method analysis to study vertical surface transport in water around 4°C. Experiments were conducted with a 30.5-cm-high heated surface. Both unidirectional and bidirectional flows were observed, precluding a unified integral method for these processes. The results of Gebhart and Mollendorf [1] indicate that choosing conventional profiles is unrealistic for some such flows.

Qureshi and Gebhart [7] measured transport from a vertical, 1.305-m-high uniform flux surface in pure water at 4°C. The input heat flux q'' was in the range 368–3617 W m^{-2}. Surface temperature measurements were made using embedded thermocouples. Fine thermocouple and hot film sensors were used for measuring velocity and temperature in the boundary region. Measurements in laminar flows were in good agreement with the similarity solution of Qureshi and Gebhart [8]. Mean and disturbance data in the unstable and transition regimes were also obtained and compared with the linear stability analysis of Qureshi and Gebhart [9], with excellent agreement.

NOMENCLATURE

c''	thermal capacity of surface per unit area exposed to fluid
g	acceleration due to gravity
Gr_L	Grashof number
k	thermal conductivity of fluid
L	length of surface
Nu_L	Nusselt number
Pr	Prandtl number of fluid
q	exponent in the density equation; 1.894816 for pure water at 1 bar
q''	surface heat flux
Q^*	$c''[g\hat{\alpha}q''^q\nu^{(q+1)}/k^{(2q+3)}]^{(1/q+3)}$
R	$(t_m-t_\infty)/(t_o-t_\infty)$
R^*	$(t_m-t_\infty)/(t_o-t_\infty)_0$
R_{1D}	$(t_m-t_\infty/[\nu^2q''^3/g\hat{\alpha}k^3]^{1/(q+3)}$
t	fluid temperature
t_L	height-averaged surface temperature
t_o	local surface temperature
x	vertical coordinate.
Δx	length of visualized portion of surface

Greek symbols

$\hat{\alpha}$	coefficient in density equation
ν	kinematic viscosity of fluid
ϕ	nondimensional temperature function
τ	physical time
τ_c	time for first departure from short time transport.

Subscripts

o	value at the surface
∞	value in the ambient
m	value at the density extremum
0	value when $t_\infty = t_m$
1	first-order correction, when $t_\infty \neq t_m$.

Higgins and Gebhart [10] carried out a similar experimental investigation with an isothermal surface. Fluid velocity and temperature measurements in the laminar regime were found to be in good agreement with the similarity solution of Gebhart and Mollendorf [1]. Mean and disturbance profiles in unstable flows were compared with predictions of the linear stability calculations of Higgins and Gebhart [11]. Again good agreement was found.

Joshi and Gebhart [12] report visualizations of plume flows above a horizontal wire energy source, for conditions in which the density extremum arose. Centerline temperature decay and velocity measurements across the plume, at $t_\infty = 4°C$, were in good agreement with the similarity solution of Mollendorf *et al.* [13]. For $t_\infty > 4°C$, the results were compared with the perturbation analysis of Gebhart *et al.* [14]. Good agreement was found for small deviations from 4°C. For $t_\infty < 4°C$, very complicated bidirectional flows were seen, at various heating rates.

All of the above studies dealt with transport in the steady state. Subsequently, Joshi and Gebhart [15] calculated the short time transient flow response adjacent to a suddenly heated vertical surface in cold water. The transient surface conditions used were: (a) a step in surface energy generation rate; and (b) a step in surface temperature.

This paper is an account of transport regimes which arise in transients adjacent to a vertical surface. The surface is subjected to a sudden, and thereafter constant, input energy generation rate q''. The surface temperature responses found in the present study are qualitatively seen in Fig. 1. In Fig. 1(a), the ambient temperature is below the extremum. Initially, for $\tau < \tau_2$, the buoyancy force is downward everywhere. Only for $\tau \geqslant \tau_2$ does an upward buoyancy force develop near the surface. Further out from the surface, the buoyancy force still remains downward, resulting in a bidirectional distribution. In Fig. 1(b), for $t_\infty > t_m$, the buoyancy force is always upward across the entire flow region.

Transient and steady surface temperature measurements were made in the range $1.2 \leqslant t_\infty \leqslant 6.8°C$. The input surface energy generation rates were in the range 587–1870 W m^{-2}. Time evolution of the resulting flows was visualized for different ambient temperature levels, all lower than t_m, the density extremum temperature. Surface temperatures are compared with the analysis in ref. [15], to determine the time intervals in the actual transients in which short time, one-dimensional solutions accurately predict actual response.

2. EXPERIMENTAL SETUP

The experimental apparatus is described in detail in Joshi [16]. The vertical surface consists of two 0.038-mm-thick Inconnel 600 foils separated by layers of resin-impregnated fabric. The resulting thickness of the composite surface is 0.28 mm, i.e. 0.011 in. Copper–constantan thermocouples (0.05 mm in diameter) were embedded between the layers of the fabric. The thin surface structure results in a very low thermal capacity and also minimizes lag in thermocouple response.

The experiment was carried out in an insulated stainless-steel tank of dimensions $1.83 \times 0.662 \times 1.83$ m high. Glass windows permit visualization of the flow from outside. The tank was filled with deionized and demineralized water, to reduce leakage of electrical current from the surface and sensors. The free surface of water was covered with Teflon-coated rafts, to reduce heat exchange and water contamination.

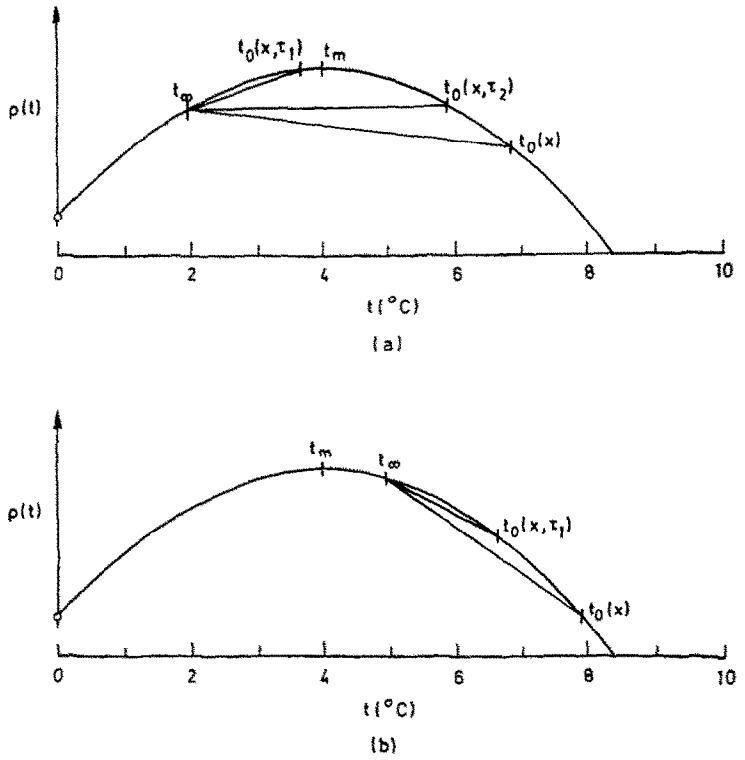

FIG. 1. Qualitative buoyancy force responses in the present study, following a sudden and constant rate of thermal energy generation within the surface. (a) $t_\infty < t_m$ and (b) $t_\infty > t_m$.

The tank walls were insulated by a 2.5-cm-thick Styrofoam, covered with an outer 10-cm layer of fiberglass insulation.

Temperature data were obtained digitally, through a Hewlett-Packard Data Acquisition System consisting of a 3497A scanner, 3456A programmable digital voltmeter and 9845B microcomputer. The scanned data were stored on magnetic tapes for subsequent processing.

Flow visualization was provided by finely ground Pliolite particles in the water. This material has a specific gravity of 1.026, which results in a large suspension time in water. The flow visualization technique is shown in Fig. 2. A 5-mW helium–neon laser beam is spread into a vertical diverging plane, or curtain, of light, perpendicular to the plane of the surface. This is achieved using a cylindrical lens. The Pliolite particles scatter the laser light into the otherwise dark background. Time exposure photographs were taken using a Nikon F3 35-mm camera with a motor drive and intervalometer, using Kodak Tri-X 400 ISO film.

Before each run, the tank water was cooled to the required temperature level, t_∞, by two Blue-M circulating chillers; the water was continuously stirred. The chillers and the stirrer were then turned off and the tank water was allowed to stand for approximately 45 min, to achieve quiescence. Test times of 30 min could be obtained without appreciable stratification in the tank. Stratification, as monitored by a vertical thermocouple array, was less than 0.15°C over the tank height at the end of all experiments.

A step in the surface energy generation rate was approximated by passing an electrical current from a 0–100 A, 0–100 V Hewlett-Packard 6475C DC power supply. The power supply was warmed for 30 min on a dummy load of approximately the same resistance as that of the test surface. Surface heating was initiated by switching the current from the dummy load. The data scanning was started before switching. Visualizations and photography were started simultaneously with the heating of the surface.

3. FLOW VISUALIZATION

As shown in ref. [15], short time transient response depends on the ambient temperature t_∞ and the imposed surface flux q''. The 12 experiments in the present study are listed in Table 1. Three heating rates were used throughout: $q'' = 587$, 1140 and 1870 W m^{-2}, at different ambient temperatures. These conditions result in both unidirectional and bidirectional buoyancy force and flow in the water. If t_∞ is greater than t_m, upflow would result at all times in the entire flow region. Thus, transient development would resemble that for conditions in which the Boussinesq approximations apply. Therefore, the only flow regimes discussed here are for $t_\infty < t_m$, at various heating levels.

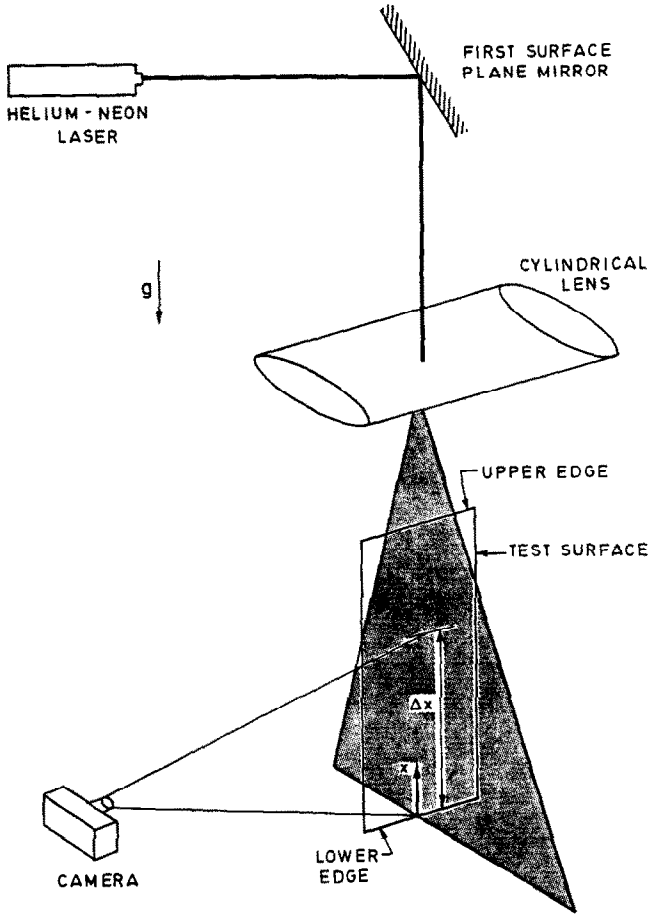

FIG. 2. Schematic sketch of the flow visualization technique.

3.1. *Steady flow regimes*

The coordinate system used in the following discussion is seen in Fig. 2, where x is always measured upward from the lower edge of the heated surface independent of actual flow direction. The distance from the leading edge of the flow pattern is denoted by X. For upflows, the lower surface edge is the leading edge. It is the trailing edge for downflows.

Table 1. Experimental conditions for the present study

Experiment	t_∞ (°C)	q'' (W m^{-2})	Q^*	R_{1D}	τ_c (s)
1	1.2	587	0.79	1.27	203
2	1.2	1140	1.02	0.85	90
3	1.2	1870	1.24	0.62	50
4	2.0	587	0.77	0.88	92
5	2.0	1140	1.00	0.58	44
6	2.0	1870	1.21	0.43	26
7	3.1	587	0.76	0.42	24
8	3.1	1140	0.98	0.28	13
9	3.1	1870	1.19	0.21	9
10	4.2	587	0.62	−0.10	0
11	5.7	587	0.60	−0.88	0
12	6.8	587	0.58	−1.47	0

Visualizations of the eventual steady flow, for the nine experiments in which $t_\infty < t_m$ are shown in Fig. 3. For $t_\infty = 1.2$°C and the lowest heat rate, 587 W m^{-2}, in Fig. 3(a), there is a large negative buoyancy force in the outer thermal region. Resulting flow response in the upper part of the picture, above the location of the arrow, is of a boundary region type. Ambient fluid rises and is then entrained. For $x < 25$ cm, below the arrow in Fig. 3(a), the flow undergoes transition to turbulence.

Figure 4 shows the same flow as in Fig. 3(a), much closer to the upper surface edge, for $30 < x < 89$ cm. Since the upper edge is the leading edge for these conditions, this corresponds to $38 < X < 97$ cm. A localized region of upflow is seen at the location of the arrow at $x = 42$ cm. The other image in all the visualizations results from reflection from the mirror-like foil surface. The strong outer downflow bends around the upflow region. This upflow is due to the buoyancy force changing direction near the surface. This is because $t_o(X) > t_m$ for sufficiently large X. However, such upflow always occurs as isolated intermittent pockets inside the more vigorous downflow further out.

Doubling the heating rate, still at $t_\infty = 1.2$°C,

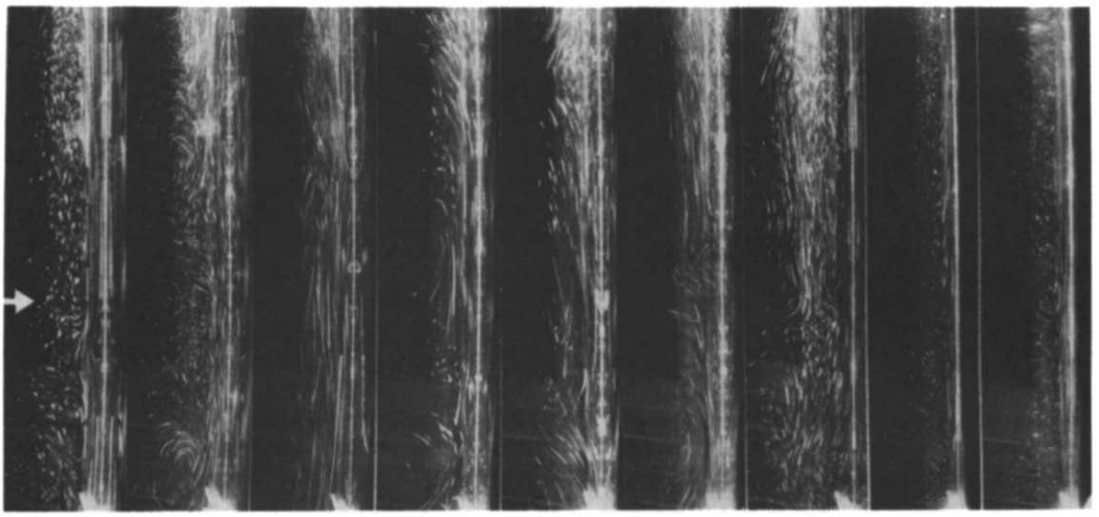

FIG. 3. Flow patterns observed in steady state for various $t_\infty < t_m$ and q''. Values of t_∞ (°C), q'' (W m^{-2}) and Δx (cm) are: (a) 1.2, 587, 58; (b) 1.2, 1140, 59; (c) 1.2, 1870, 59; (d) 2.0, 587, 66; (e) 2.0, 1140, 66; (f) 2.0, 1870, 66; (g) 3.1, 587, 56; (h) 3.1, 1140, 75; and (i) 3.1, 1870, 73.

results in a thick turbulent downflow region, Fig. 3(b). Very close to the surface, a much weaker and intermittent upflow is seen. A similar flow pattern arises for a further 50% increase in q'' as seen in Fig. 3(c). The local upflow occurred more frequently in time than before in Fig. 3(b), and at more locations along the surface. This arises from a stronger upward buoyancy force as $t_o(X)$ increases more rapidly downstream. Thus it exceeds t_m by a larger amount and produces a larger inside buoyancy force reversal.

Flow patterns for $t_\infty = 2.0$°C are seen in Figs. 3(d)–(f), at the three heating rates. A turbulent outer downflow exists for all three heating levels. The inner upflow, which is intermittent for the lowest heating rate, Fig. 3(d), is continuous at the higher rates in Figs. 3(e) and (f).

For a still higher ambient temperature, $t_\infty = 3.1$°C, the flow patterns are seen in Figs. 3(g)–(i). A developing upflow region becomes clearly established near the surface even at the lowest heating rate, Fig. 3(g). The outer downflow in Fig. 3(g) developed late in the transient. This is discussed further in connection with the transient flow development in Section 3.2.

For large x, the outer downflow mixes with the thickened inner upflow. This results in the formation of the distinct counterclockwise vortices, seen in Fig. 5. These vortices are convected along the surface. At higher heating rates, for $t_\infty = 3.1$°C, Figs. 3(h) and (i) show very regular upward flow near the surface. The outer downflow bringing in entrainment, is much weaker than in Fig. 3(g). These patterns changed with time.

These visualizations illustrate the many mechanisms which result from the buoyancy and flow reversals over the ambient temperature range, from 1.2°C to near the extremum, at $t_\infty = 3.1$°C, for increasing rates of heating. The transient evolution to such flows is considered next.

3.2. *Transient flow development*

Similar time exposure photographs during the transient evolution, from quiescence, are shown in Figs. 6–9. For all conditions of t_∞ and q'', a one-dimensional flow regime was seen at short times, as calculated in ref. [15]; departure from this kind of response occurs later. These calculations indicate that two different mechanisms of entrainment development occur. If t_∞ is far away from t_m, the flow is unidirectional; entrainment development starts from the leading edge. On the other hand, in a bidirectional flow, much more complex entrainment development mechanisms arise. The visualizations also show that strongly bidirectional transient flows are very unstable. Some become turbulent even before entrainment has developed along the entire surface.

For $t_\infty < t_m$, the thermal input first results in a downward buoyancy force, see Fig. 1(a). This gives rise to an initial downflow. Later, an upflow develops near the surface and the flow becomes bidirectional. The calculations of Joshi and Gebhart [15] determine when the inner upflow arises. The surface thermal capacity effect indicated by the parameter Q^*, was included in these calculations. These times are listed in Table 1, as τ_c, for the experimental conditions here.

3.2.1. *Flow development at low ambient temperatures.* Transient flow development for the lowest t_∞ and q'', 1.2°C and 587 W m^{-2}, is seen in the time

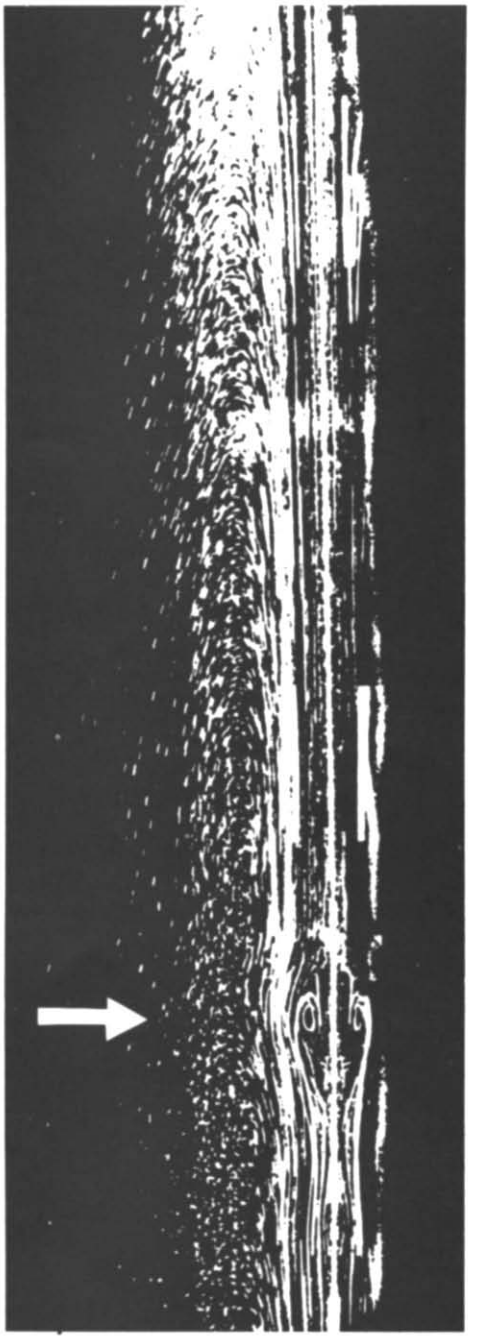

FIG. 4. Downward boundary region like flow for $t_\infty = 1.2°C$ and $q'' = 587\ W\ m^{-2}$ in the range $30 < x < 89$ cm. A localized upflow region exists at $x = 42$ cm.

FIG. 5. Steady flow pattern for $t_\infty = 3.1°C$ and $q'' = 587\ W\ m^{-2}$ in the range $57 < x < 118$ cm. A strong outer downflow is observed. Inner upflow entrains in the form of discrete vortices.

sequence in Figs. 6(a)–(g), for $0 < x < 57$ cm. The first effect is a one-dimensional downflow, seen in (a). Entrainment into this flow is seen in (b) near the top. It has developed all the way down to the lower edge in (c), at about 208 s. A clockwise vortex has appeared near the top in (d). In (e), this first vortex has moved downward and a second vortex is visible above it. Later, in (f), both vortices have moved downward and reached the lower edge of the surface. A completely downward boundary region flow is now established. Later, in (g) localized regions of intermittent inner upflow have developed, near the surface. This is seen in (g) at approximately mid-height. The downward flow bends around this region, as also seen earlier in Fig. 4. Entrainment pattern near the lower edge of the surface, in (g), appears irregular, indicating transition. This is supported by surface temperature measurements discussed later.

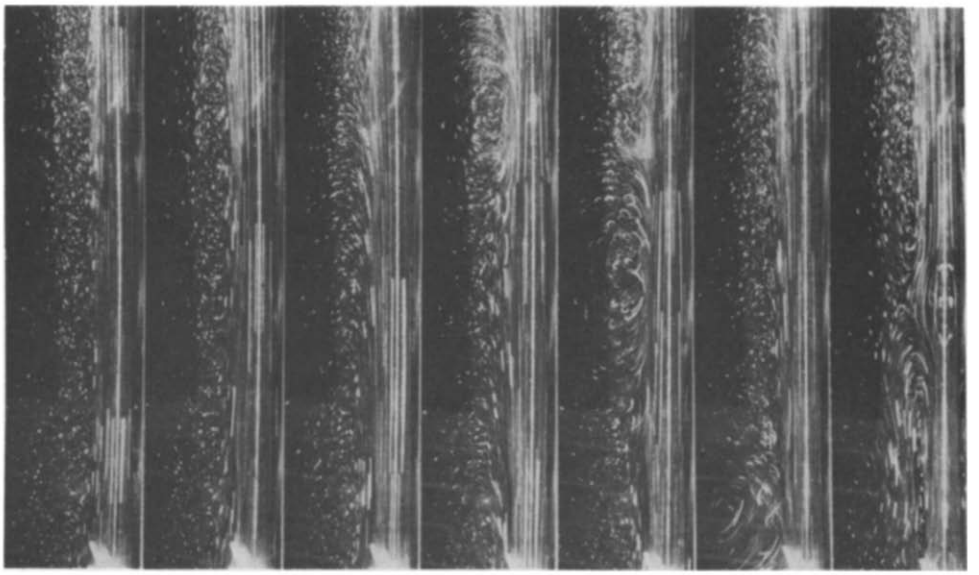

(a) (b) (c) (d) (e) (f) (g)

FIG. 6. Transient flow development for $t_\infty = 1.2°C$ and $q'' = 587$ W m^{-2} in the range $0 < x < 57$ cm. Exposure durations in seconds are: (a) 110–130; (b) 154–174; (c) 198–218; (d) 220–240; (e) 242–262; (f) 396–416; and (g) 704–724.

The flow development, again at $t_\infty = 1.2°C$, but at the intermediate heating rate of 1140 W m^{-2} is seen in Figs. 7(a)–(g). It is similar until late in the transient. A one-dimensional downflow is again seen in (a) and (b). Again the development of entrainment starts from the upper edge, as seen in (c). The one-dimensional calculations predict the first occurrence of upflow, near the surface, at $\tau_c = 90$ s, see Table 1. In Fig. 7(c), after the onset of bidirectional flow, downward and upward developing entrainment patterns are seen at

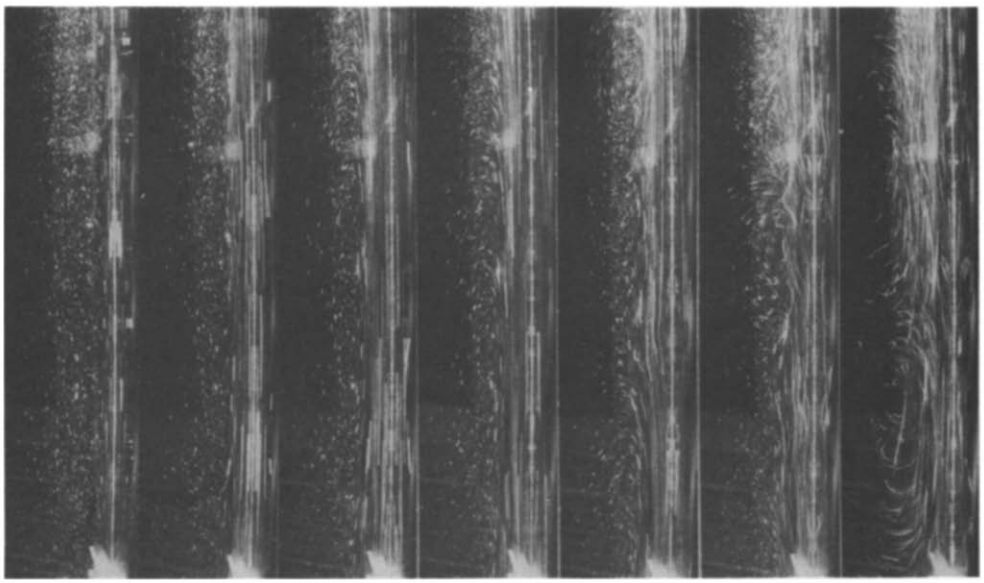

(a) (b) (c) (d) (e) (f) (g)

FIG. 7. Transient flow development for $t_\infty = 1.2°C$ and $q'' = 1140$ W m^{-2} in the range $0 < x < 60$ cm. Exposure durations in seconds are: (a) 32–52; (b) 98–118; (c) 142–162; (d) 164–184; (e) 186–206; (f) 208–228; and (g) 296–316.

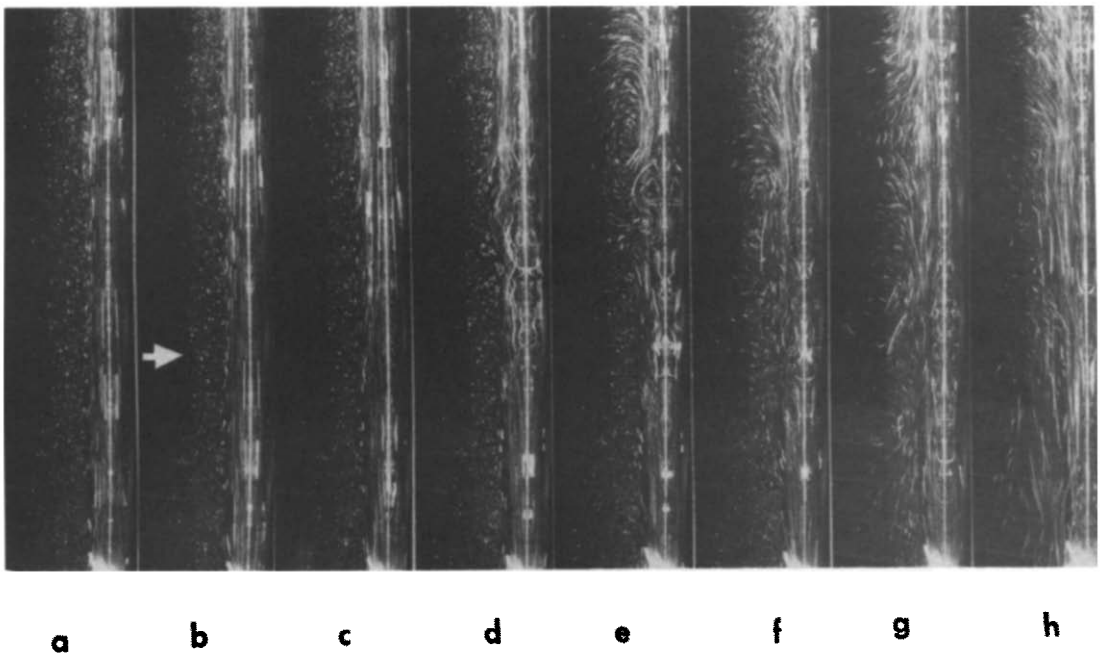

FIG. 8. Transient flow development for $t_\infty = 1.2°C$ and $q'' = 1870$ W m^{-2} in the range $0 < x < 62$ cm. Exposure durations in seconds are: (a) 67–82; (b) 86–101; (c) 105–120; (d) 124–139; (e) 143–158; (f) 162–177; (g) 181–196; and (h) 238–253.

the top and bottom, respectively. The developing entrainment at the bottom is seen to be suppressed in (d). This may be due to the increasing and stronger outer downflow. In (e) and (f), highly amplified disturbances are seen. The flow becomes turbulent later, in (g).

A quite different flow response arises at a yet higher heating level, as seen in Figs. 8(a)–(h). Initial one-dimensional downflow is seen in (a). The calculation indicates first inner upflow at about 50 s. Later, in (b), this upflow has become stronger, causing upward developing entrainment up to the location of the arrow. In (c), disturbances are seen near the surface at mid-height. They amplify at later times and in (h) the flow is completely turbulent. The flow has become turbulent before any entrainment has arisen at the upper edge.

The responses for the two higher heating rates in Figs. 7 and 8, are very different than for the lower heating rates in Fig. 6. In Fig. 7, the flow is purely downward and laminar for $\tau < 130$ s and has a developing boundary region characteristic. Later an upflow develops and causes entrainment development at the bottom of the surface. The flow later undergoes transition. In Fig. 8, upflow appears much earlier, at $\tau = 50$ s. Downward entrainment does not develop before the entire flow undergoes transition to turbulence. At the two higher heating rates, the resulting bidirectional flow increases velocity gradients and local shear stress across the flow region. The instabilities may arise from this.

The transient flow evolutions seen at an ambient temperature of 2.0°C for the same three heating rates, were similar to Figs. 7 and 8. For $q'' = 587$ W m^{-2}, the lowest heating, bidirectional entrainment development occurred followed by transition, as in Fig. 7. The two higher heating rates showed flow patterns similar to those in Fig. 8.

3.2.2. *Transient flows with ambient temperatures just below* t_m. A further increase in ambient temperature, to 3.1°C, results in a much weaker early outer downward buoyancy force. The resulting very long and complicated response at the lowest heating rate is seen in Figs. 9(a)–(g). An early inner upflow near the surface, in (a), results in entrainment development starting from the bottom edge of the surface, in (b). Later, in (c), a well defined and thin upward laminar developing flow is established.

This flow then undergoes drastic changes, due to a number of interacting effects. First, the heated wake shed above the top edge of the surfaces mixes with ambient at 3.1°C. This results in more dense water downstream, that is, above the surface. This water sinks downward, as seen clearly already in (d). The average velocity of the leading front of the downflow is about 2 mm s^{-1}. This downflow continues at an approximately constant rate, in (e)–(g).

For the two higher heating rates 1140 and 1870 W m^{-2}, at $t_\infty = 3.1°C$, the outer downward flow was much weaker than seen in Fig. 9. The eventual flows for these conditions were shown in Figs. 3(h) and (i). They resemble upward developing boundary region flow.

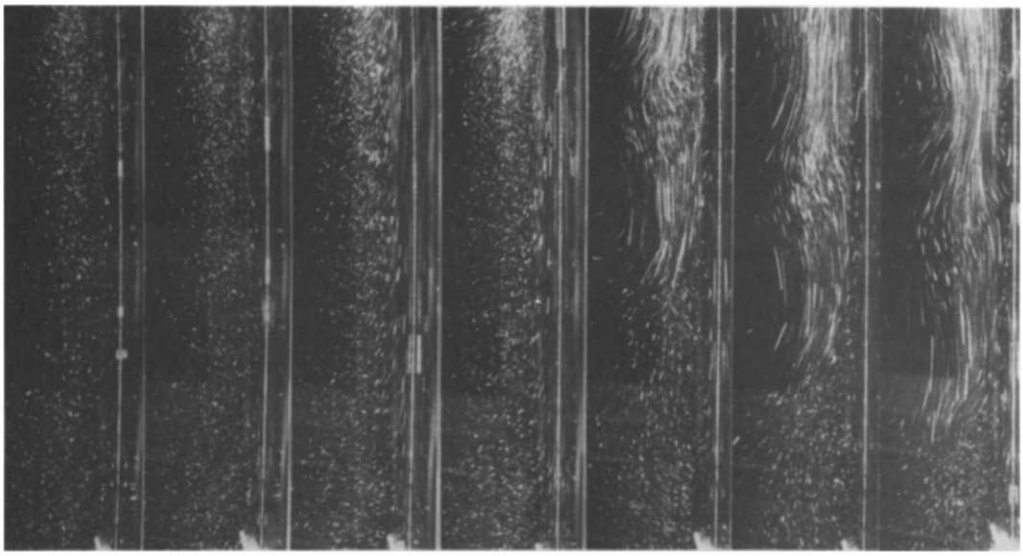

FIG. 9. Transient flow development for $t_\infty = 3.1°C$ and $q'' = 587$ W m^{-2} in the range $0 < x < 55$ cm. Exposure durations in seconds are: (a) 102.5–122.5; (b) 143.5–163.5; (c) 369–389; (d) 492–512; (e) 615–635; (f) 656–676; and (g) 697–717.

4. SURFACE TEMPERATURE MEASUREMENTS

Temperatures were measured along the surface, both during the transient, and in steady state, for all conditions in Table 1. These temperature responses confirm the flow development mechanisms elaborated in Section 3. The measurements in the eventual established flow are discussed first. Then their transient evolution is considered.

4.1. *Steady surface temperatures*

As seen in Section 3, reversals in the direction of buoyancy force and flow occur across the range of t_∞. These changes in flow regimes and heat transfer are also documented by measurements of average local surface temperature, $t_o(x)$. These are discussed next, in Figs. 10–14. To compute $t_o(x)$, averaging times of 400 s or more were used, whenever the steady temperatures showed disturbance levels of 5% or more from the mean.

4.1.1. *Local measurements at various ambient temperatures.* Figure 10 shows the average surface temperature distributions, along the surface, for ambient temperatures of 1.1, 2.0, 3.1, 4.2, 5.7 and 6.8°C, for the lowest heating rate of 587 W m^{-2}. Unfilled symbols correspond to laminar flow states and filled symbols are for disturbance levels of 5% or more around the mean. For the lowest ambient temperature, $t_\infty = 1.2°C$, a primarily downward flow exists. Recall Figs. 3(a) and 4. The leading edge for this flow is the upper surface edge. The surface temperature in Fig. 10 increases downstream from the leading edge as the flow region thickens. Transient temperature traces for these conditions are seen in Fig. 11. The measurements imply laminar flow response at $x = 96.8$ and 70.0 cm. Larger fluctuations arise further downstream, as the flow undergoes transition to turbulence.

For the ambient at 2.0°C, turbulent downflow was seen in Fig. 3(d). Figure 10 shows only small variations in the surface temperature at the various x levels. Local temperature responses for these conditions are seen in Fig. 12. Disturbance amplitudes from the mean are 5% or more at all locations.

An increase in the ambient temperature to 3.1°C resulted in upflow near the surface, as seen in Figs. 3(g) and 5. The corresponding temperature levels in Fig. 10 increase with x, for $0 < x < 54.5$ cm. Downstream, at larger x, the flow undergoes transition. Temperature traces with time in Fig. 13 show some fluctuations even for $x < 49.0$ cm. These appear to be caused by the unsteady nature of the outer downflow, seen in Figs. 3(g) and 5. The disturbance amplitudes increase downstream and higher frequency components appear, indicating transition to turbulence.

For $t_\infty \geqslant 4.0°C$, upflow occurs for all x, although these conditions do not result in a steady, self-similar solution for the transport. For t_∞ near t_m, a perturbation analysis has been carried out in ref. [14]. The following expression for the surface temperature distribution is derived from these results.

$$(t_o - t_\infty) = [1 + (qR^*)\phi_1(0, Pr)] \times \frac{q''x\sqrt{2}}{(gx^3\hat{\alpha}/\nu^2)^{1/4}k[-\phi'(0, Pr)]}. \quad (1)$$

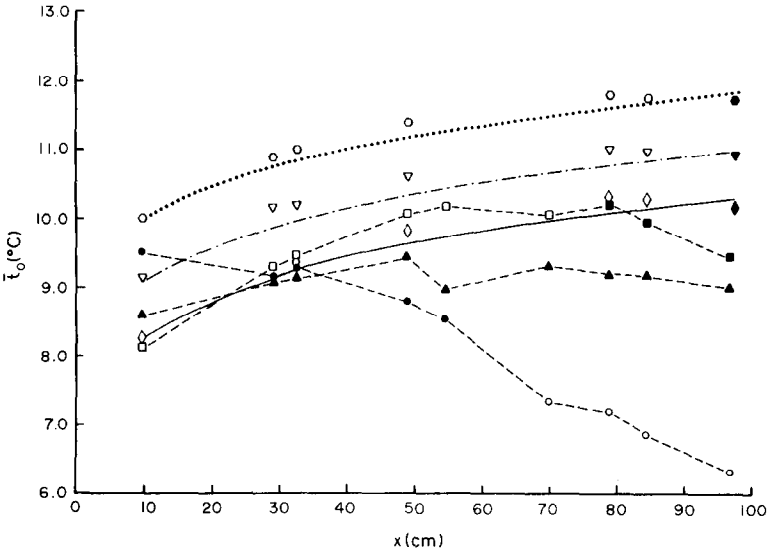

FIG. 10. Steady mean local surface temperatures, $\bar{t}_0(x)$, for $q'' = 587$ W m^{-2} at various t_∞; ○ 1.2°C, △ 2.0°C, □ 3.1°C, ◇ 4.2°C, ▽ 5.7°C, and ⬡ 6.8°C. Solid symbols indicate fluctuation levels of 5% or more from the mean. Dashed lines join data points for ambient temperatures for which no analysis exists. —— Analysis of Gebhart *et al.* [14]; — · — · — similarity solution with Boussinesq approximations for $Pr = 10.0$ at $t_\infty = 5.7$°C; · · · · same as — · — · — at $t_\infty = 6.8$°C.

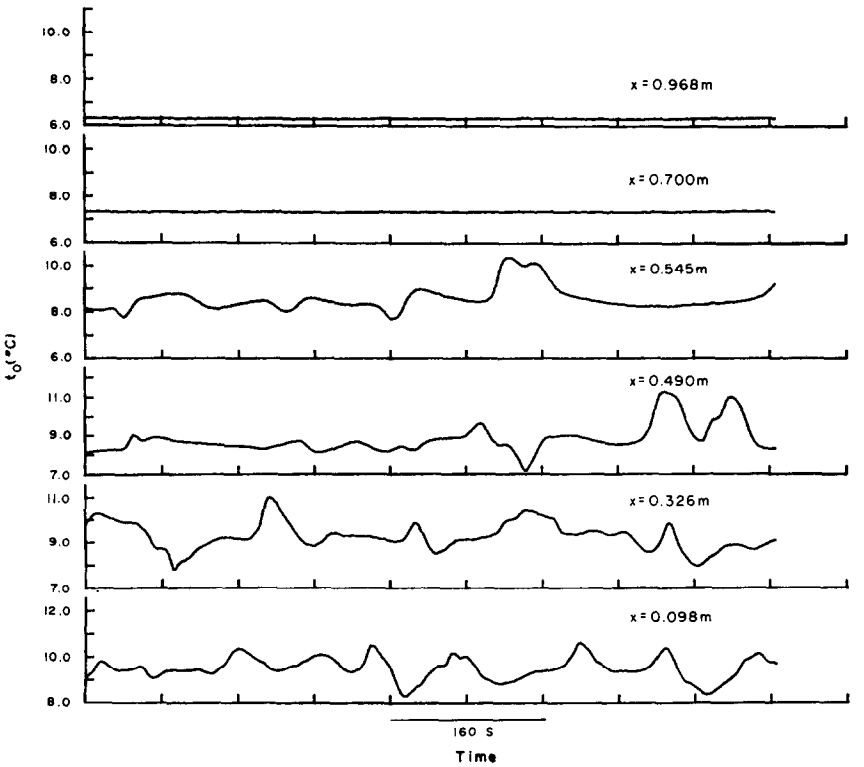

FIG. 11. Local temperature spectra at various x after steady conditions have been achieved for $q'' = 587$ W m^{-2} and $t_\infty = 1.2$°C.

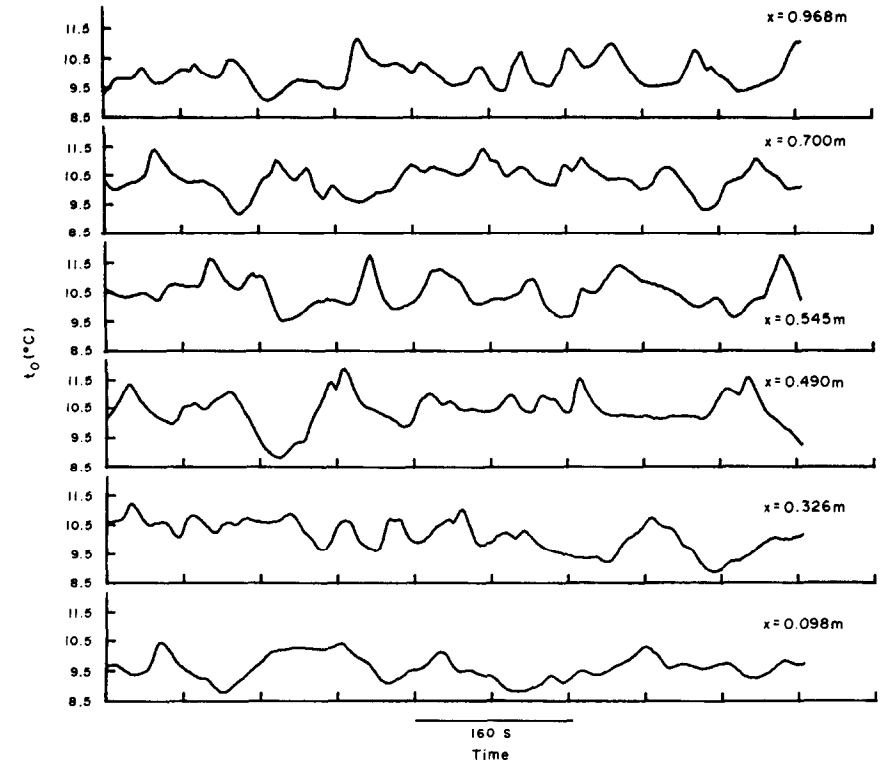

FIG. 12. Local temperature spectra at various x after steady conditions have been achieved for $q'' = 587$ W m^{-2} and $t_\infty = 2.0$°C.

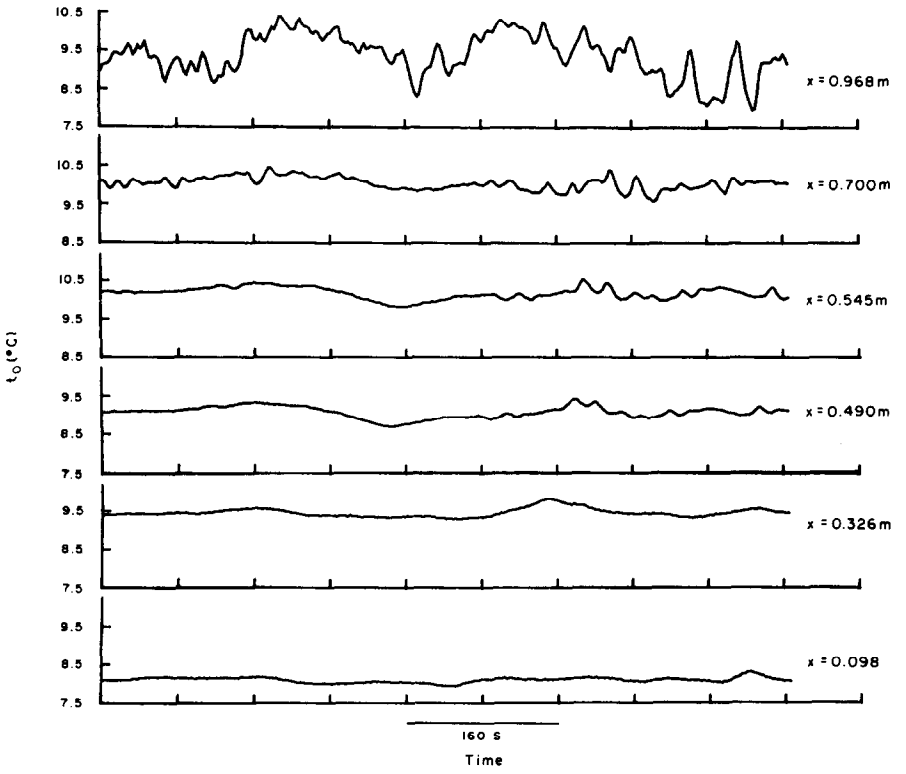

FIG. 13. Local temperature spectra at various x locations after steady conditions have been achieved for $q'' = 587$ W m^{-2} and $t_\infty = 3.1$°C.

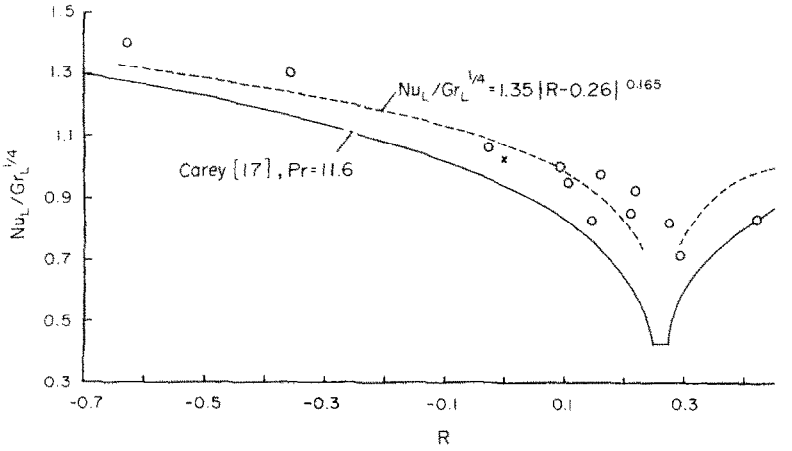

FIG. 14. Variation of $Nu_L/Gr_L^{1/4}$ with R. Solid line is the correlation of Carey [17] for vertical, isothermal surfaces in cold water. Data points are shown as circles. The single point shown as × corresponds to the similarity analysis for $t_\infty = 4.0°C$ from Gebhart and Mollendorf [1]. Dashed line is the proposed correlation.

In equation (1), qR^* characterizes departures from the similarity condition of $t_\infty = 4.0°C$ and is given by $R^* = (t_m - t_\infty)/(t_o - t_\infty)_0$ where $(t_o - t_\infty)_0$ is the surface temperature response from ref. [1]. For $Pr = 11.6$, $\phi_1(0) = 0.41024$ and $-\phi'(0) = 1.16529$. Notice that $R^* = 0$ when $t_\infty = t_m$. For pure water at 1 bar, $\hat{\alpha} = 9.297173 \times 10^{-6}(°C)^{-q}$ and $q = 1.894816$.

In Fig. 10, good agreement exists between equation (1) and the data for $t_\infty = 4.2°C$ in the laminar region. The surface temperature decreases instead, beyond 80 cm, with transition. For $t_\infty = 5.7$ and 6.8°C, equation (1) becomes invalid since (qR^*) is no longer small. Data for these conditions were compared with the Boussinesq calculation for a constant flux surface at $Pr = 10.0$. All properties were evaluated at a film temperature corresponding to this value of Pr. The Boussinesq analysis overpredicts the buoyancy force for these conditions, yielding lower temperatures than measured. Surface temperature data decrease for $x > 80$ cm, with transition.

4.1.2. *Nusselt number correlation.* In any practical application, the overall Nusselt number is a quantity of great importance. Time-averaged local surface temperatures, $\bar{t}_o(x)$, were also spatially averaged at nine locations along the surface. This surface height averaged temperature $\bar{t}_L$ was then used in the calculation of the Grashof number, $Gr_L = [g\hat{\alpha}|t_L - t_\infty|^q L^3/\nu^2]$, and the parameter $R = (4.0 - t_\infty)/(t_L - t_\infty)$. The Nusselt number was calculated as $Nu_L = q''L/[k(t_L - t_\infty)]$.

The resulting Nusselt number data, in the form of $Nu_L/Gr_L^{1/4}$ as a function of R, are plotted in Fig. 14. Also shown is the correlation curve due to Carey [17] for vertical, isothermal surfaces in cold water. For $Pr = 11.6$ it is given by:

$$Nu_L/Gr_L^{1/4} = 1.39|R-0.26|^{0.242}. \quad (2)$$

Most of the present data points fall above the correlation, as does the single point corresponding to $R = 0$ from the similarity solution in ref. [1].

A new correlation was therefore developed on the present data, for a uniform flux condition. The data, outside the range $0.23 < R < 0.29$ are well correlated by

$$Nu_L/Gr_L^{1/4} = 1.35|R-0.26|^{0.165}. \quad (3)$$

This result is also in better agreement with the calculation for $R = 0$.

A minimum in heat transfer arises within the range $0.23 < R < 0.29$. Based on the data of Ede [4] for a 10.2-cm-high surface, Carey [17] suggests an approximately constant value for $Nu_L/Gr_L^{1/4}$ for these conditions.

Our data near $R = 0.29$ for a much higher surface show largely turbulent flow and a resulting small variation in surface temperature along the surface as seen in Fig. 12. For a uniform input flux condition, this implies $Nu_L/Gr_L^{1/4}$ proportional to $L^{1/4}$. Thus a surface height dependence on heat transfer is indicated. This dependence is also supported by the data in ref. [4]. The ratio $[L/L_{Ede}]^{1/4}$ is 1.87, which is within 11% of the measured ratios of the minimum $Nu_L/Gr_L^{1/4}$ in the two studies.

4.2. *Transient surface temperature response*

Surface temperatures during the transient confirm the short time response calculated in ref. [15]. The data also indicate the mechanisms of transport departure from one dimensional. These are described next in Figs. 15–18, across the range of ambient conditions and thermal inputs.

Figure 15 shows the local surface temperature response at $x = 9.8$ cm for different ambient temperatures, in the range 1.2–6.8°C, for $q'' = 587$ W m^{-2}. The solid line is the one-dimensional conduction solution for negligible surface thermal capacity. As seen in ref. [16], this is a very good approximation for the thin surface used in the present experiments. The surface temperature response for these conditions is

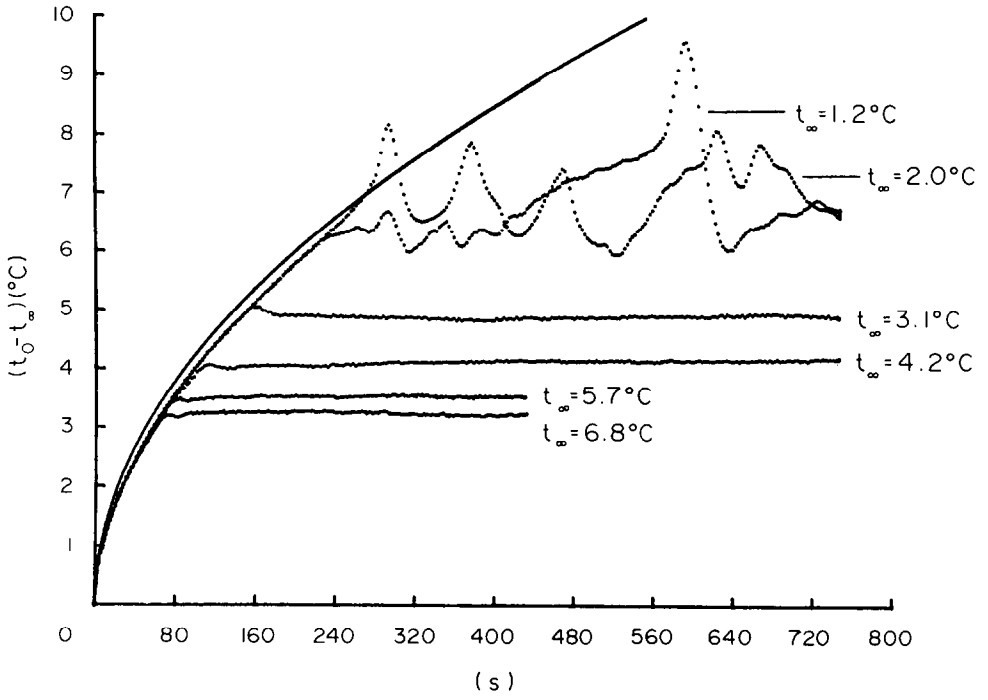

FIG. 15. Transient surface temperature development for various t_∞, for $q'' = 587$ W m^{-2} at $x = 9.8$ cm. The solid line is equation (4).

calculated simply as

$$(t_o - t_\infty) = \frac{2q''}{k}\left[\frac{\alpha\tau}{\pi}\right]^{1/2}. \quad (4)$$

For the highest ambient temperature, $t_\infty = 6.8$°C, measured response follows equation (4) for $\tau < 70$ s. Steady state is later achieved rapidly. Lower levels of t_∞, 5.7°C and 4.2°C, result in progressively delayed departures from the one-dimensional trend during the transient; also, the eventual surface temperatures are higher. These departure times are collected in Table 2. For $t_\infty > t_m$, entrainment development always starts from the leading edge and progresses downstream with time.

The local buoyancy force levels are reduced as t_∞ is decreased towards the extremum temperature. For a given q'', the reduced buoyancy force levels result in weaker flow velocities during the transient. One-dimensional transport at a given x location, therefore, continues for a longer time. Also, reduced flow velocities result in poorer heat transfer and consequently higher steady surface temperatures above the ambient, for a given heat flux input.

As the ambient temperature is reduced below 4°C, the initial flow is downward. For sufficiently large q'', the flow becomes bidirectional. For $t_\infty = 3.1$°C, in Fig. 15, the one-dimensional transport persists to about $\tau = 160$ s. A 7% temperature overshoot occurs just before steady state is reached. As seen from Table 2, for $x = 9.8$ cm, the entrainment development from the lower edge first terminates one-dimensional transport.

Reducing the ambient temperature to 2.0°C prolongs one-dimensional transport. For $t_\infty = 1.2$°C, the large downward buoyancy force dominates the flow. As seen in Fig. 3(a), and also from Table 2, one-dimensional transport terminates with the arrival of disturbances from the leading edge. For these conditions it is the upper surface edge.

Transient response near the top of the surface, at $x = 96.8$ cm, is seen in Fig. 16 for the same conditions as in Fig. 15. No extremum arises for ambient temperatures of 6.8, 5.7 and 4.2°C; all three responses are similar. The initial conduction response is followed by a decrease in temperature level. Later, the surface temperatures increase again to achieve steady state. This trend is different from those in Fig. 15. No similar drop in the surface temperature during the transient was observed close to the leading edge.

Transient experiments in room temperature water, reported in ref. [16], show identical behavior. Laminar mechanisms persist for all times near the leading edge, causing no decrease in surface temperature. However, the transient flow undergoes transition downstream. The enhanced transport results in a temporary drop in the surface temperature. Later, the flow partially relaminarizes. Then the surface temperatures increase to the eventual steady-state levels. These temperatures are lower than the calculations in ref. [14], due to transition.

For $t_\infty = 3.1$°C, in Fig. 16, disturbances from the upper edge of the surface terminate the one-dimensional transport. As seen from Table 2, the longest duration of one-dimensional transport does not occur

Table 2. Measured first departure times in seconds from one-dimensional transport

Experiment	x (cm) 9.8	29.0	32.6	49.0	54.5	70.0	79.0	84.4	96.8
1	248	220	216	196	192	162	150	144	120
2	160	188	200	214		136	128	120	100
3	93	107		110	115	110	109	113	115
4	260	324	334	230	220	196	180	172	140
5	120	130	144	156	160	160	146	150	150
6	75	103	104	104	108	96	100	90	98
7	156	220	220	230	245	252	238	238	204
8	88	128	134	132	138	148	142	138	136
9	58	87	90	96	96	100	100	90	90
10	80	140	150	180	186		200	205	216
11	76	112	116	138	142		154	160	166
12	70	105	106	120	124		140	144	150

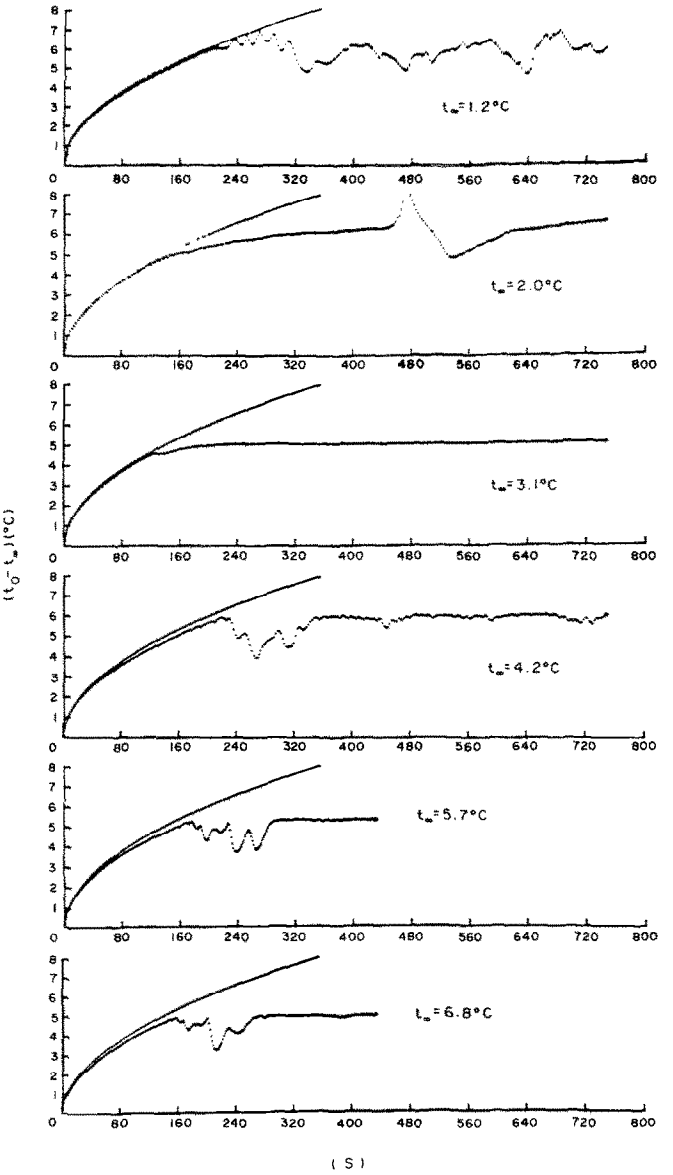

FIG. 16. Transient surface temperature development for identical conditions as in Fig. 15 at $x = 0.968$ m. The solid line is equation (4).

either near the upper or the lower edge of the surface; rather it occurs between. This results from the bidirectional entrainment development. At ambient temperatures of 2.0°C and 1.2°C, the departure from the conduction trend occurs earlier. The strong early downflow for these conditions carries the upper edge disturbances at faster rates.

Figures 15 and 16 explain the transient transport development mechanisms across a range of ambient temperatures, for $q'' = 587$ W m^{-2}. Different q'', for a given t_∞ have complex effects on transport development. For $t_\infty > t_m$, increasing q'' yields higher buoyancy force and flow velocities, causing earlier departures from the conduction trend and a faster achievement of steady state for a given $t_\infty < t_m$. Increasing q'' also results in an earlier establishment of bidirectional flow. As observed in Section 3, these bidirectional flows later become turbulent. This is confirmed by surface temperature measurements in Fig. 17 for $q'' = 1870$ W m^{-2} at $t_\infty = 1.2$°C. Data are plotted for four x locations. One-dimensional transport persists for $\tau < 110$ s. Later, disturbances appear at all four x locations almost simultaneously. Steady temperature data show large fluctuations from the mean, indicating turbulent transport. Flow visualization sequences for these conditions in Fig. 8 support these mechanisms.

The unstable flow behavior seen in Fig. 17 does not occur at higher ambient temperatures. This is seen in Fig. 18, for $t_\infty = 3.1$°C and $q'' = 1870$ W m^{-2}.

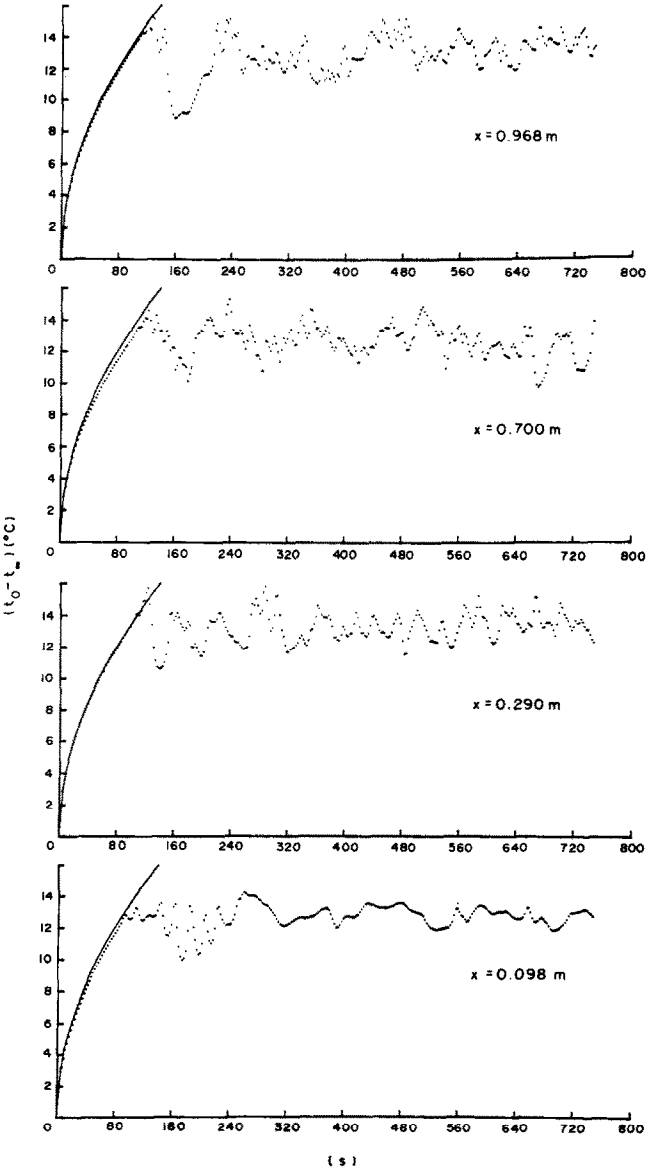

FIG. 17. Transient surface temperature development for $q'' = 1870$ W m^{-2} and $t_\infty = 1.2$°C at various x.

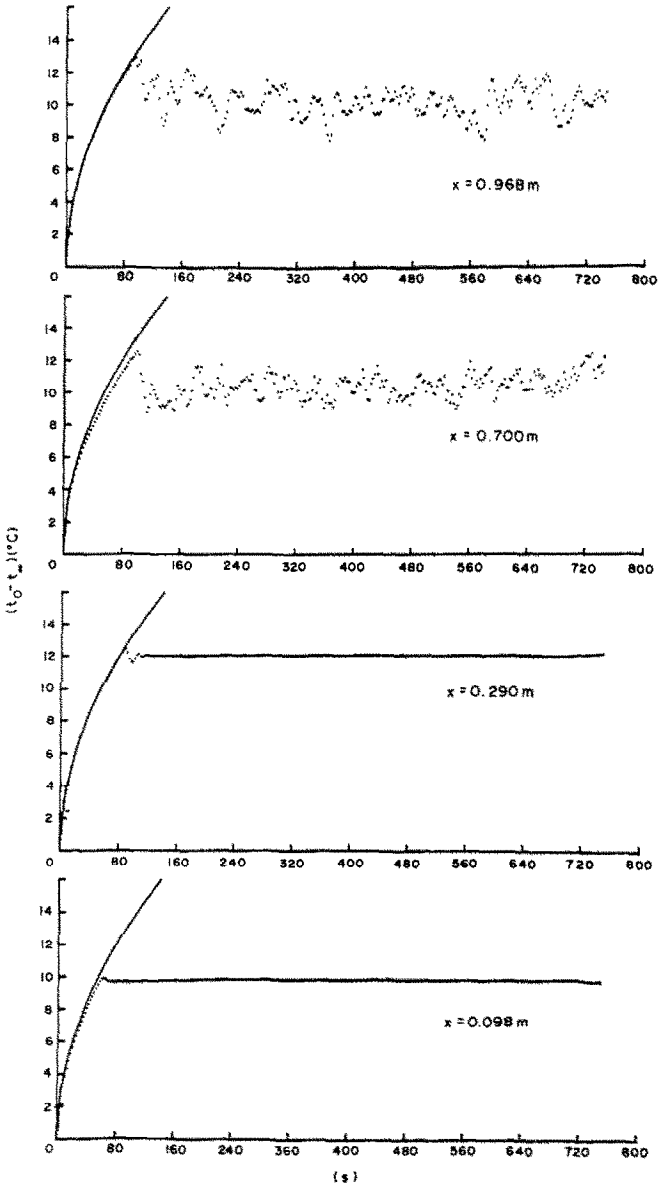

FIG. 18. Transient surface temperature development for $q'' = 1870$ W m^{-2} and $t_\infty = 3.1$°C at various x.

At higher ambient temperatures there is a faster establishment of upflow than in Fig. 17. The outer downflow is weaker. The flow development then resembles that of an upward boundary region. Thermocouples at $x = 9.8$ cm and $x = 29.0$ cm show laminar flow mechanisms for all times. Transition to turbulence occurs for $x = 0.70$ m and $x = 0.968$ m.

5. CONCLUSIONS

Time exposure photographs and surface temperature measurements presented here explain the transport development adjacent to a suddenly heated, vertical surface in cold water. For $t_\infty < 4.0$°C, the initial one-dimensional flow is downward. This flow for low q'' develops entrainment downward from the upper edge of the surface, resulting in a developing boundary region flow. Increasing t_∞ or q'' causes transient bidirectional flow. Such flows were found to be unstable, resulting ultimately in a strong turbulent downflow away from the surface. A weak intermittent upflow was seen very close to the surface.

Further increase in t_∞ to near 4.0°C causes an even stronger inner upflow. The outer downflow is then only intermittent. It arises because the warmer wake shed above the top edge of the surface mixes with colder ambient to produce denser water. This water then sinks, altering the initially established boundary region structure. Increased levels of q'' result in much weaker and intermittent outer downflow.

Correlations for steady heat transfer data have been obtained. Transient temperature measurements confirm an initially diffusive transport regime. Departure times from such one-dimensional characteristic have been determined. Analytical predictions for entrainment development in transient bidirectional flows do not exist at present. Our measurements of the transient transport will be useful in any such modelling efforts.

Acknowledgements—The authors acknowledge support for this study through NSF grant MEA 82 17756. Discussions with Dr B. Sammakia were held at various stages. The expert efforts of Ms Claudia McNeill in the preparation of the manuscript are acknowledged.

REFERENCES

1. B. Gebhart and J. C. Mollendorf, Buoyancy-induced flows in water under conditions in which density extrema may arise, *J. Fluid Mech.* **89,** 673–707 (1978).
2. B. Gebhart and J. C. Mollendorf, A new density relation for pure and saline water, *Deep Sea Res.* **24,** 831–848 (1977).
3. V. P. Carey and B. Gebhart, Visualization of the flow adjacent to a vertical ice surface melting in pure cold water, *J. Fluid Mech.* **107,** 37–55 (1981).
4. A. J. Ede, The influence of anomalous expansion on the thermal convection in water, *Appl. scient. Res.* **5,** 458–460 (1955).
5. H. J. Merk, The influence of melting and anomalous expansion on the thermal convection in laminar boundary layers, *Appl. scient. Res.* **4,** 435–452 (1953).
6. R. S. Schechter and H. S. Isbin, Natural-convection heat transfer in regions of maximum fluid density, *A.I.Ch.E. Jl* **4,** 81–89 (1958).
7. Z. H. Qureshi and B. Gebhart, Measurements of fluid and thermal transport in vertical buoyancy induced flows in cold water, *Int. J. Heat Mass Transfer* **24,** 1503–1512 (1981).
8. Z. H. Qureshi and B. Gebhart, A new formulation for buoyancy induced flow adjacent to a vertical uniform flux surface in cold water, *Numer. Heat Transfer* **2,** 467–476 (1979).
9. Z. H. Qureshi and B. Gebhart, The stability of vertical buoyancy induced flows in cold pure and saline water, *Int. J. Heat Mass Transfer* **29,** 1383–1392 (1986).
10. J. M. Higgins and B. Gebhart, Measurements of instability and disturbance growth in vertical buoyancy induced flows in cold water, *Int. J. Heat Mass Transfer* **25,** 1397–1409 (1982).
11. J. M. Higgins and B. Gebhart, The stability of vertical buoyancy induced flow in cold water, *Trans. Am. Soc. mech. Engrs*, Series C, *J. Heat Transfer* **105,** 767–773 (1983).
12. Y. Joshi and B. Gebhart, An experimental study of plane plumes in cold water, *Trans. Am. Soc. mech. Engrs*, Series C, *J. Heat Transfer* **105,** 248–254 (1983).
13. J. C. Mollendorf, R. S. Johnson and B. Gebhart, Several constant energy plume flows in pure and saline water at its density extremum, *J. Fluid Mech.* **113,** 269–282 (1981).
14. B. Gebhart, V. P. Carey and J. C. Mollendorf, Buoyancy induced flow due to energy sources in cold quiescent pure and saline water, *Chem. Engng Commun.* **3,** 555–575 (1979).
15. Y. Joshi and B. Gebhart, Vertical transient natural convection flows in cold water, *Int. J. Heat Mass Transfer* **27,** 1573–1582 (1984).
16. Y. Joshi, Transient natural convection flows in water and natural and mixed convection flows in porous media. Ph.D. thesis, University of Pennsylvania (1984).
17. V. P. Carey, A heat transfer correlation for natural convection from a vertical surface in cold water, *Trans. Am. Soc. mech. Engrs*, Series C, *J. Heat Transfer* **105,** 658–660 (1984).

MESURES ET VISUALISATIONS DE LA CONVECTION NATURELLE VARIABLE ET PERMANENTE DANS L'EAU FROIDE

Résumé—On donne les résultats d'une étude expérimentale sur la convection naturelle adjacente à une surface verticale de 1,27 m de hauteur, soudainement chauffée. Ces mesures déterminent les effets du comportement anormal de l'eau froide sur la réponse convective et sur les caractéristiques thermiques. Le domaine des températures ambiantes étudié est $1{,}2 \leqslant t_\infty \leqslant 6{,}8°C$, pour des flux de chaleur entre 587 et 1870 W m^{-2}. L'écoulement variable et stationnaire est visualisé et les températures locales de température sont mesurées. Pour les conditions de la plus basse température ambiante et de chauffage, $t_\infty = 1{,}2°C$ et 587 W m^{-2}, l'écoulement établi ressemble à une couche limite d'écoulement descendant. Quand t_∞ et le flux de chauffage augmentent l'écoulement n'a pas de forme simple: on voit une descente fortement turbulente loin de la surface et une montée intermittente très près de la surface. Un accroissement ultérieur de t_∞ et du flux de chauffage renforce l'écoulement ascendant. Le mouvement externe descendant existe toujours, néanmoins il est intermittent pour $t_\infty = 3{,}1°C$ et 1140–1870 W m^{-2}. Dans ces conditions, les écoulements ressemblent à une couche limite montante. La température moyennée sur la hauteur t_L est utilisée dans l'évaluation du Nu_L et Gr_L près de la température extrémale t_m. L'état stationnaire est bien représenté par $Nu_L/Gr_L^{1/4} = 1{,}35\,[R-0{,}26]^{0{,}165}$ hors de $0{,}23 < R < 0{,}29$ où $R = (t_m-t_\infty)/(t_L-t_\infty)$. A l'intérieur de $0{,}23 < R < 0{,}29$ on observe un minimum du transfert thermique. Les mesures montrent les changements qualitatifs dans les régimes d'écoulement et aussi la variation du nombre de Nusselt dans la région de l'extremum de densité. Ces caractéristiques sont nettement différentes de celles trouvées dans le comportement bien étudié de Boussinesq.

MESSUNGEN UND SICHTBARMACHUNG VON INSTATIONÄREN UND STATIONÄREN VERTIKALEN KONVEKTIONSSTRÖMUNGEN IN KALTEM WASSER

Zusammenfassung—Es werden Ergebnisse der experimentellen Untersuchung von instationären natürlichen Konvektionsströmungen und Transportvorgängen in kaltem Wasser bei einer sprungartigen Beheizung einer 1,27 m hohen vertikalen Oberfläche dargestellt. Diese Messungen zeigen den Einfluß des anomalen Verhaltens von kaltem Wasser auf die instationäre Ausbildung der Konvektion und auf die Wärmetransportcharakteristik im stationären Endzustand. Der Bereich der Umgebungstemperatur beträgt $1{,}2 \leqslant t_\infty \leqslant 6{,}8°C$, und der Bereich der Heizwärmestromdichte 587–1870 W m^{-2}. Die transiente und die stationär sich einstellende Strömung wurden sichtbar gemacht, und die lokalen Oberflächentemperaturen wurden gemessen. Für die kleinste Umgebungstemperatur und Heizleistung ($t_\infty = 1{,}2°C$ und 587 W m^{-2}) hat die eingesetzte Strömung Ähnlichkeit mit einer abwärts strömenden Grenzschicht. Bei Anstieg der Temperatur t_∞ und der Heizleistung hat die Strömung nicht die Form einer einfachen Grenzschicht. Es wurde eine lebhafte turbulente Abwärtsströmung in einiger Entfernung von der Oberfläche und eine intermittierende Aufwärtsströmung an der Oberfläche beobachtet. Ein weiterer Anstieg der Temperatur t_∞ und der Heizleistung erzeugt stärkere innere Aufwärtsströmungen. Die äußere Abwärtsströmung existiert zu jeder Zeit. Jedoch stieg sie nur zeitweise für $t_\infty = 3{,}1°C$ und Heizleistungen von 1140 bis 1870 W m^{-2} an. Diese Wechsel im Transportvorgang werden durch lokal gemessene Oberflächentemperaturen bestätigt. Die über der Oberflächenhöhe gemittelte Temperatur t_L wurde in die Berechnung von Nu_L und Gr_L nahe der Maximaltemperatur t_m eingesetzt. Die mittleren stationären Wärmeübergangsdaten können außerhalb von $0{,}23 < R < 0{,}29$ am besten mit der Beziehung $Nu_L/Gr_L^{1/4} = 1{,}35|R-0{,}26|^{0{,}165}$ wiedergegeben werden, wobei $R = (t_m - t_\infty)/(t_L - t_\infty)$ ist. Im Bereich $0{,}23 < R < 0{,}29$ wurde ein Minimum des Wärmeübergangs beobachtet. Details der Entwicklung der Strömung während der instationären Phase werden ebenfalls von Beginn an untersucht.

ИЗМЕРЕНИЯ И ВИЗУАЛИЗАЦИЯ ПЕРЕХОДНОГО И УСТАНОВИВШЕГОСЯ ВЕРТИКАЛЬНОГО ЕСТЕСТВЕННО-КОНВЕКТИВНОГО ТЕЧЕНИЯ В ХОЛОДНОЙ ВОДЕ

Аннотация—Представлены результаты экспериментального изучения переходного и развитого естественно-конвективного течения, обусловленного внезапным нагреванием вертикальной пластины высотой 1,27 м в холодной воде. С помощью измерений определено влияние аномального поведения холодной воды на конвективные переходные характеристики и установившиеся характеристики теплопереноса. Температура окружающей среды—$1{,}2 \leqslant t_\infty \leqslant 6{,}8°C$, интенсивность теплоподвода—587–1870 Вт/м^2. Наблюдались переходное и установившееся течения; измерялись локальные температуры поверхности. Для наименьших температуры окружающей среды $t_\infty = 1{,}2°C$ и условий нагрева 587 Вт/м^2 установившееся течение напоминало стекающий пограничный слой. С ростом t_∞ и интенсивности нагрева течение видоизменялось. Замечено сильное турбулентное, направленное вниз течение вдали от поверхности и ячеистое восходящее около нее. Дальнейшее увеличение интенсивности нагрева ведет к более сильным восходящим внутренним течениям. Наружное нисходящее течение существует при всех условиях. Однако при $t_\infty = 3{,}1°C$ и скоростях нагрева 1140 и 1870 Вт/м^2 оно возникает скачкообразно. Для этих условий течение напоминает восходящий пограничный слой. Эти изменения в режиме переноса подтверждены измерениями локальной температуры поверхности. Осредненная по высоте температура поверхности t_L использовалась для оценки Nu_L и Gr_L вблизи экстремума температуры t_m. Осредненные данные по установившемуся теплопереносу наилучшим образом обобщаются с помощью выражения $Nu_L/Gr_L^{1/4} = 1{,}35|R - 0{,}26|^{0{,}115}$ за пределами $0{,}23 < R < 0{,}29$, где $R = (t_m - t_\infty)/(t_L - t_\infty)$. В диапазоне $0{,}23 < R < 0{,}29$ наблюдается минимальная интенсивность теплопереноса. Также изучаются детали развития течения и переноса при переходном режиме, начиная с устойчивого состояния. Вначале за одномерным кондуктивным переносом следует режим развития течения. В зависимости от условий нагрева окружающей среды и поверхности наблюдались однонаправленный и двунаправленный режимы развития течения. Найдено, что двунаправленные переходные течения неустойчивы и приводят к турбулентному течению. Переход к турбулентности происходит одновременно на всем участке вниз по потоку. Сохранение одномерного переноса было определено в разных точках вниз по потоку для всех условий нагрева и температуры окружающей среды. Измерения показывают качественные переходы в режимах течения, а также изменение во времени числа Нуссельта в области экстремального значения плотности. Полученные характеристики полностью отличаются от найденных в случае хорошо изученных течения и теплообмена в приближении Буссинеска.